ELSEVIER

Physica B 289–290 (2000) 326–330

PHYSICA B

www.elsevier.com/locate/physb

Magnetism of thin chromium films studied with low-energy muon spin rotation

H. Luetkens[a,b,*], J. Korecki[c,d], H. Glückler[b], E. Morenzoni[b], T. Prokscha[b], A. Schatz[a], M. Birke[a], E.M. Forgan[e], B. Handke[c], A. Hofer[b,f], T.J. Jackson[e], M. Kubik[c], F.J. Litterst[a], Ch. Niedermayer[f], M. Pleines[b,f], T.M. Riseman[e], G. Schatz[f], T. Slezak[c], H.P. Weber[b]

[a]*Institut für Metallphysik und Nukleare Festkörperphysik, Technische Universität Braunschweig, D-38106 Braunschweig, Germany*
[b]*Paul Scherrer Institut, Labor für Myonenspinspektroskopie, CH-5232 Villigen PSI, Switzerland*
[c]*Faculty of Physics and Nuclear Techniques, Academy of Mining and Metallurgy, PL-30-059 Kraków, Poland*
[d]*Institute of Catalysis and Surface Chemistry, Polish Academy of Science, PL-30-059 Kraków, Poland*
[e]*School of Physics and Astronomy, University of Birmingham, Birmingham B15 2TT, UK*
[f]*Fakultät für Physik, Universität Konstanz, D-78457 Konstanz, Germany*

Abstract

Low-energy muon spin rotation (LE-μ^+SR) measurements were performed on 3.4 and 9.1 nm epitaxial Cr(0 0 1) films buried by non-magnetic boundary layers to study the collapse of the spin-density wave (SDW) of bulk Cr, which is expected when decreasing the thickness of the film below the modulation period of the SDW (≈ 6 nm). Magnetic phases of Cr are identified by the fast relaxation of the muon spin polarization. While a reduced Néel temperature of 285 K with respect to the bulk value is found for the 9.1 nm Cr layer, the 3.4 nm film remains in a magnetic phase over the investigated temperature range of 20–320 K.

PACS: 75.30.Fv; 75.70.Cn; 76.75.+i

Keywords: Thin films and multilayers; Low-energy μSR; Magnetism

1. Introduction

The magnetism of bulk Cr was intensively investigated in the last decades (for a review see Ref. [1]). Below the Néel temperature of $T_N = 311$ K an incommensurate SDW is formed with the antiferromagnetic ordered Cr moments showing spatial sinusoidal modulation. Recently, the magnetic structure of thin Cr films has attracted much interest because of the giant magneto resistance observed in Fe/Cr multilayers. In these materials, Cr acts as a mediating spacer between the exchange coupled Fe layers. Finite thickness of the Cr layer, proximity to the ferromagnetic Fe layers and spin frustration at rough interfaces have considerable effect on the Cr magnetism [2–10]. By reducing the

*Correspondence address. Paul Scherrer Institut, WLGA/B15, CH-5232 Villigen PSI, Switzerland. Tel.: +41-563-104-275; fax: +41-563-103-294.

E-mail address: hubertus.luetkens@psi.ch (H. Luetkens).

0921-4526/00/$ - see front matter
PII: S0921-4526(00)00403-8

Cr thickness t_{Cr} in these multilayers, T_N decreases and finally drops to zero at a critical thickness $t_0 \approx 4.2$ nm which is close to the modulation period of the SDW. This is well described by the scaling theory assuming a magnetically dead layer of thickness t_0 below which the incommensurate SDW does not fit into the Cr layer anymore [2]. However, contradictory opinions about the magnetic state of Cr below t_0 can be found in the literature. Paramagnetic [3] as well as commensurate antiferromagnetic behaviour [4] up to 500 K have been observed. For $t_0 < t_{Cr} < 25$ nm perturbed angular correlation (PAC) spectroscopy finds the Cr to be in a longitudinal SDW state with the chromium spins directed out of the film plane and an enhanced $T_N = 525$ K [3]. In the same thickness region, neutron-scattering experiments [5] show a transverse SDW with the spins in the film plane and a reduced T_N due to the size effect [6]. These contradictory results follow from the strong dependence of the magnetic structure on various parameters, especially on specific structural properties resulting from different sample preparation conditions.

Another approach to the problem is to first study the intrinsic magnetic properties of thin Cr films buried by non-magnetic boundary layers. For $t_{Cr} < 25$ nm this has only been done for Ag/Cr multilayers with the PAC method [11]. In these multilayers, Cr remains in the longitudinal SDW phase up to a temperature of 500 K. Below a critical thickness of 5.1 nm the collapse of the SDW and a transition to paramagnetic behaviour is observed.

Following this approach, two different Cr samples were prepared with non-magnetic boundary layers: one with $t_{Cr} = 3.4$ nm and another with $t_{Cr} = 9.1$ nm in order to cover both interesting regions below and above the collapse of the SDW.

2. Sample preparation and measurements

Samples were grown in an UHV system equipped with MBE, LEED and AES which ensured a base pressure below 10^{-10} hPa and a pressure during the deposition in the low 10^{-10} hPa range. All samples were evaporated on $10 \times 10 \times 1$ mm^3 MgO(0 0 1) plates, cleaved from blocks prior to introduction into the UHV system. After annealing in UHV for 1 h at 620°C the substrates revealed a clean MgO(0 0 1) surface as checked by AES and LEED. Chromium films and sandwiches were grown on buffer layers deposited on the MgO substrate in a multi-stage process at an evaporation rate of about 0.5 nm/min. First, a thin (usually 4 nm) Cr(0 0 1) seed-layer was grown directly on MgO at about 100°C, followed by a 17 nm Au layer at 180°C. This base layer was annealed for 1 h at 520°C and finally a 3 nm Au layer was added at 180°C. The resulting 28×5 Au(0 0 1) reconstructed surface (Au(0 0 1)-hex) is characterized by low roughness due to monoatomic steps only, and reconstruction ridges in two perpendicular domain directions [12]. Au(0 0 1)-hex surface is a good template for growing flat Fe films [12,13] for which a layer-by-layer growth mode is promoted by Au surfactant action. A similar effect is expected for Cr, being isostructural with Fe. Although STM observation of Cr growth on Au(0 0 1)-hex has not been reported, from the very similar results of the LEED analysis of Cr and Fe on Au(0 0 1)-hex we expect the same growth mode. Fig. 1 presents a LEED pattern for a 9.1 nm Cr(0 0 1) film deposited on the Au(0 0 1)-hex surface at 150°C. Narrow spots at in-phase diffraction conditions (e.g. 87 eV), much

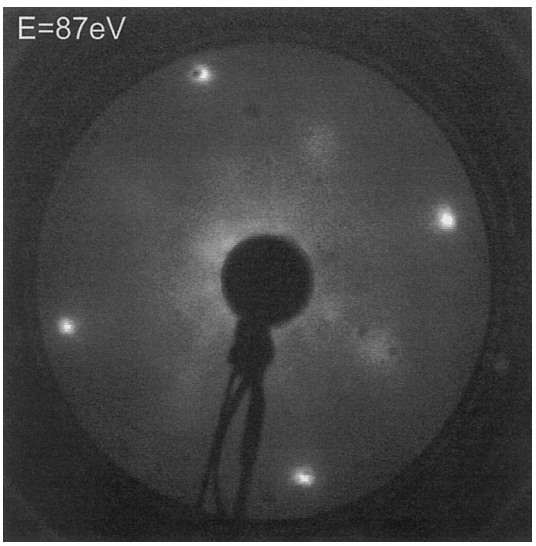

Fig. 1. LEED pattern of a 9.1 nm thick Cr(0 0 1) film on a Au(0 0 1)-hex surface.

narrower than those for the Cr seed-layer, become broadened at out-of-phase conditions as expected for monoatomic roughness. Gold, when grown on such Cr(0 0 1) surfaces at 150°C, reveals again a perfect Au(0 0 1)-hex surface, which is restored after few Au atomic layers. Thus, high-quality Cr/Au sandwiches and superlattices can be grown. Two samples, coated eventually with Al cap layers were prepared. Their thickness, with a typical uncertainty of 5%, was determined during evaporation by using a quartz microbalance. An additional inhomogeneity of the order of 5% of the thickness results from the oblique deposition. Finally, we performed X-ray reflectometry measurements, which gave the following layer sequences in nanometers: Sample 1: MgO(0 0 1)/3.4(3) Cr/21.3(4) Au/9.1(4) Cr/34.5(9) Al, Sample 2: MgO(0 0 1)/4.3(3) Cr/21.4(3) Au/3.4(3) Cr/10.2(3) Au/3.4(4) Cr/35.0 (9) Al, where the numbers in parentheses denote the mean roughness.

These samples were investigated with LE-μ^+SR [14] using the LE-μ^+ beam at the Paul Scherrer Institut, Switzerland. We performed zero field (ZF) and transverse field (TF) measurements in a temperature range of 20–320 K. In the case of TF measurements magnetic fields of 5–10 mT were applied parallel to the incoming muon beam, i.e. perpendicular to the initial muon spin polarization and to the film surface. For a detailed description of the sample region of the LE-μSR apparatus we refer to Ref. [15]. The muon implantation energy (E_{impl}) was tuned between 1.8–29.3 keV. This allows to vary the ratio of muons stopping in the relevant Cr and in the non-magnetic boundary layers. The muon implantation depths were determined by the Monte Carlo code TRIM.SP [16], which has proven to be suitable for calculating LE-μ^+ implantation profiles in solids [17].

3. Results and discussion

In Fig. 2, the typical time evolution of the reduced asymmetry in ZF and TF measurements on the 9.1 nm Cr sample is shown. These data were taken at 150 K with $E_{\mathrm{impl}} = 7.4$ keV at which about 30% of the muons come to rest in the 9.1 nm Cr layer. The ZF spectrum was fitted by a superposition of two exponentially damped signals yielding relaxation rates of $\lambda_{\mathrm{fast}} = 10.8 \pm 3.9\ \mu\mathrm{s}^{-1}$ and $\lambda_{\mathrm{slow}} = 0.17 \pm 0.03\ \mu\mathrm{s}^{-1}$. The amplitude of the fast decaying signal corresponds approximately to the fraction of muons stopping in Cr which, at this temperature, is expected to be in the SDW state. The large relaxation rate is then due to a broad field distribution at the muon site. The weakly damped fraction of the spectrum represents muons stopping in the non-magnetic layers of the sample.

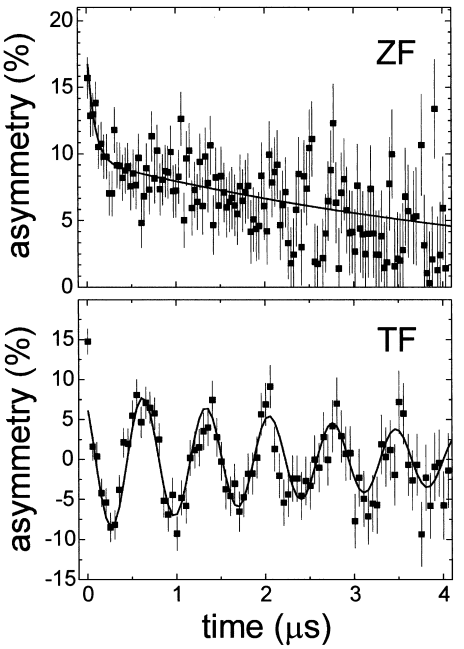

Fig. 2. ZF and TF reduced asymmetries obtained with the 9.1 nm Cr sample in a magnetically ordered state ($T = 150$ K, $E_{\mathrm{impl}} = 7.4$ keV).

The TF spectra can be satisfactorily fitted by a single exponentially damped precession signal with an asymmetry A_{TF} reflecting the fraction of muons which have thermalized in a non-magnetic surrounding. In the case where Cr is in a magnetically ordered state, it does not contribute to A_{TF} because of the too fast relaxation of the muon spin polarization. The observed A_{TF} is shown in Fig. 3 as a function of E_{impl} at 20 and 320 K together with simulated implantation profiles. At low E_{impl} almost all muons stop in the covering non-magnetic 34.5 nm thick Al overlayer. At 20 K, the decrease of A_{TF} with increasing E_{impl} reflects the

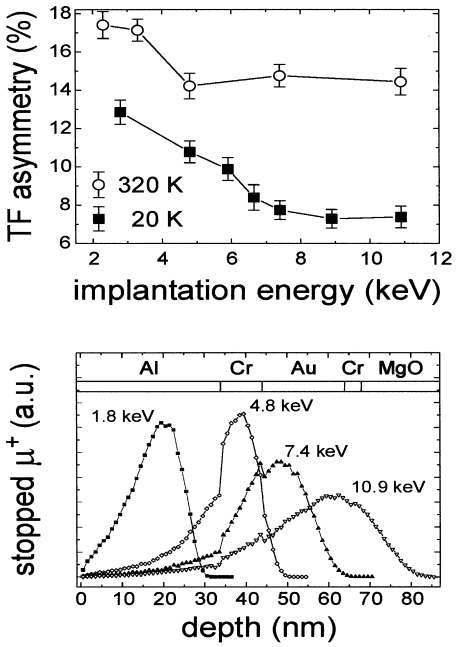

Fig. 3. (Top): Transverse field asymmetry A_{TF} as a function of E_{impl} for the 9.1 nm Cr sample. (Bottom): Calculated implantation profiles for $E_{impl} = 1.8$, 4.8, 7.4 and 10.9 keV.

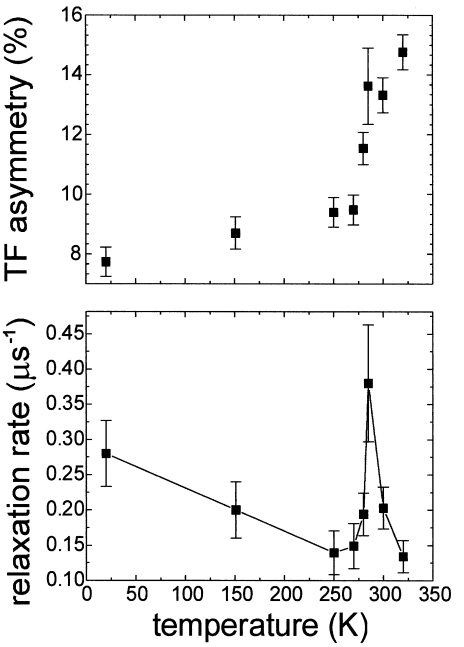

Fig. 4. Transverse field asymmetry A_{TF} and relaxation rate as a function of temperature for the 9.1 nm Cr sample measured with 7.4 keV muons.

increasing muon fraction stopping in magnetically ordered Cr. However, the drop of the asymmetry occurs at a higher energy than expected from the simulation. The reason for this discrepancy must await further investigations, clarifying the role of absorbed overlayers as of muon diffusion. At 320 K, when the muon penetrates into the 9.1 nm Cr layer, a higher asymmetry and a smaller reduction of A_{TF}, compared to the 20 K measurements, are observed. This temperature dependence of A_{TF} is illustrated in Fig. 4. The significant drop in A_{TF} associated with a peak in the relaxation rate clearly indicates the magnetic ordering of the major volume fraction of the Cr layer below $T_N = 285 \pm 5$ K.

For the 3.4 nm Cr sample we measured the energy dependence of A_{TF} at 20 and 320 K (see Fig. 5). Again, a reduction of A_{TF} with increasing E_{impl} is observed. At higher energies the fraction of muons stopping in the two 3.4 nm Cr layers increases and the decrease of A_{TF} can be attributed to the magnetic order in Cr. However, differently from the results for the thicker Cr sample, within the experimental errors, no difference between the energy scans at 20 and 320 K is observed. Thus, we find the 3.4 nm Cr layer to exhibit magnetic order over the whole investigated temperature range.

The observed commensurate antiferromagnetism for $t_{Cr} < t_0$ in Fe/Cr multilayers [4] was attributed to the proximity of the Cr to the ferromagnetic Fe. In our case, two other interpretations are possible: (i) Interfacial alloying of Al at the uppermost Cr layer could lead to commensurate antiferromagnetic order with an enhanced T_N as it is observed in bulk $Cr_{1-x}Al_x$ alloys with $x > 0.03$ [18]. From experiences with the similar Fe/Al system the intermixing does not exceed the first three atomic layers making interfacial alloying in our case not very probable. Moreover, it should be noted that the second Cr layer buried by Au should not be influenced by this effect that, at variance with our observation, A_{TF} should rise with increasing E_{impl} in a paramagnetic Cr film. (ii) The magnetism could be induced by internal strain caused by a small tetragonal distortion due to the lattice mismatch of Cr and Au. This behaviour is again in analogy with the one observed in the bulk, where

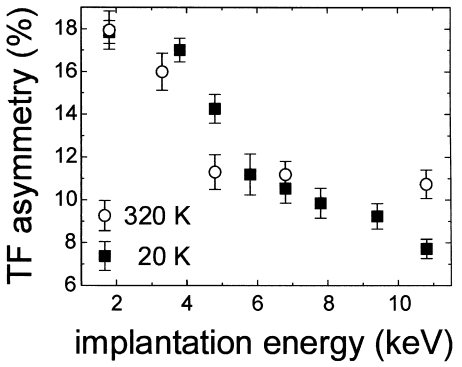

Fig. 5. Transverse field asymmetry A_{TF} as a function of E_{impl} for the 3.4 nm Cr sample at 20 and 320 K.

the antiferromagnetic order with T_N up to 450 K has been found to be associated with strain in heavily crushed Cr powder samples [1].

4. Summary

We performed LE-μ^+SR measurements on two different thin film Cr(0 0 1) samples buried by non-magnetic boundary layers. Magnetic order in Cr films is identified by a fast relaxation of the muon spin polarization leading to a reduction of the observed TF asymmetry. The fast relaxation does not allow to characterize in detail the magnetic phases with respect to orientation of the Cr spins and direction of the SDW propagation. However, the results clearly show the 3.4 nm Cr to be in a static magnetically ordered state in the temperature range from 20 to 320 K, whereas the 9.1 nm Cr sample reveals a magnetic phase transition at 285 K as concluded from a characteristic reduction of A_{TF} associated with a peak in relaxation rate at this temperature.

Acknowledgements

We gratefully acknowledge financial support from the Paul Scherrer Institut, the German BMBF and the UK EPSRC. The TRIM.SP code was kindly provided by W. Eckstein, Max Planck Institut für Plasmaphysik, Garching, Germany.

References

[1] E. Fawcett et al., Rev. Mod. Phys. 60 (1988) 209.
[2] E.E. Fullerton et al., Phys. Rev. Lett. 75 (1995) 330.
[3] J. Meersschaut et al., Phys. Rev. Lett. 75 (1995) 1638.
[4] A. Schreyer et al., Phys. Rev. Lett. 79 (1997) 4914.
[5] P. Bödeker et al., Phys. Rev. Lett. 81 (1998) 914.
[6] E.E. Fullerton et al., Phys. Rev. Lett. 77 (1996) 1382.
[7] H. Zabel et al., J. Phys. D 31 (1998) 656.
[8] P. Bödeker et al., Physica B 248 (1998) 115.
[9] P. Bödeker et al., Phys. Rev. B 59 (1999) 9408.
[10] J. Meersschaut et al., Phys. Rev. B 57 (1998) 1638.
[11] S. Demuynck et al., Phys. Rev. Lett. 81 (1998) 2562.
[12] N. Spiridis, J. Korecki, Appl. Surf. Sci. 141 (1999) 313.
[13] V. Blum et al., Phys. Rev. B 59 (1999) 15 966.
[14] E. Morenzoni, Appl. Magn. Reson 13 (1997) 219.
[15] E. Morenzoni et al., Physica B 289–290 (2000), These Proceedings.
[16] W. Eckstein, Computer Simulation of Ion-Solid Interactions, Springer, Berlin, 1991.
[17] H. Glückler et al., Physica B 289–290 (2000), These Proceedings.
[18] E. Fawcett et al., Rev. Mod. Phys. 66 (1994) 25.